INSTITUTE OF PHYSICS PUBLISHING PHYSICS IN MEDICINE AND BIOLOGY

Phys. Med. Biol. **50** (2005) 4931–4953 doi:10.1088/0031-9155/50/20/012

Anatomically constrained dipole adjustment (ANACONDA) for accurate MEG/EEG focal source localizations

Chang-Hwan Im[1,2], **Hyun-Kyo Jung**[2] **and Norio Fujimaki**[3]

[1] Department of Biomedical Engineering, University of Minnesota, 7-105 BSBE, 312 Church Street SE, Minneapolis, MN 55455, USA
[2] School of Electrical Engineering and Computer Science, Seoul National University, Shillim-dong, Kwanak-gu, Seoul 151744, Korea
[3] Brain Information Group, National Institute of Information and Communications Technology (NICT), 588-2, Iwaoka, Iwaoka-cho, Nishi-ku, Kobe, Hyougo 651-2492, Japan

E-mail: ichism@elecmech.snu.ac.kr

Received 10 May 2005, in final form 3 July 2005
Published 5 October 2005
Online at stacks.iop.org/PMB/50/4931

Abstract

This paper proposes an alternative approach to enhance localization accuracy of MEG and EEG focal sources. The proposed approach assumes anatomically constrained spatio-temporal dipoles, initial positions of which are estimated from local peak positions of distributed sources obtained from a pre-execution of distributed source reconstruction. The positions of the dipoles are then adjusted on the cortical surface using a novel updating scheme named cortical surface scanning. The proposed approach has many advantages over the conventional ones: (1) as the cortical surface scanning algorithm uses spatio-temporal dipoles, it is robust with respect to noise; (2) it requires no *a priori* information on the numbers and initial locations of the activations; (3) as the locations of dipoles are restricted only on a tessellated cortical surface, it is physiologically more plausible than the conventional ECD model. To verify the proposed approach, it was applied to several realistic MEG/EEG simulations and practical experiments. From the several case studies, it is concluded that the anatomically constrained dipole adjustment (ANACONDA) approach will be a very promising technique to enhance accuracy of focal source localization which is essential in many clinical and neurological applications of MEG and EEG.

(Some figures in this article are in colour only in the electronic version)

1. Introduction

Magnetoencephalography (MEG) and electroencephalography (EEG) are kinds of non-invasive measuring techniques to estimate and characterize neural electrical sources in a human brain (Hämäläinen *et al* 1993, Malmivuo and Plonsey 1995). MEG measures magnetic field induced from neural current flows in the cerebral cortex and EEG measures electric potential differences that the current makes on the scalp surface. Nowadays, the two similar methods have become indispensable tools for studying neural processes of the normal brain as well as treating serious neurological disorders such as epilepsy, Parkinson's disease and so on. In contrast to the other brain imaging modalities, which generally measure brain metabolism and neurochemistry, such as fMRI and PET, MEG and EEG are based on the electromagnetic phenomena of neurons, and thus they have superior temporal resolution less than several milliseconds.

The main objective of MEG and EEG inverse problems is to estimate neural current sources from external electromagnetic measurements. These kinds of inverse problems have suffered from various obstacles such as high sensitivity to noise, ill-posed characteristic, difficulty in verification and so on. To solve the problems and estimate the brain sources more efficiently, many approaches and algorithms have been studied (Baillet *et al* 2001a). Among them, two types of source models are generally used: the equivalent current dipole (ECD) model and the distributed source model. The ECD model assumes small numbers of current dipoles to approximate the flow of electrical current in a small brain area. It has been proved to be a powerful exploration tool in many cognitive and clinical applications (Ebersole 1994, de Munck *et al* 1988). The main advantages of the ECD model are that it is very simple to implement and is robust to noise. To apply the ECD model, however, the numbers of ECDs should be determined *a priori*, which is often very difficult due to lack of preliminary information. In addition, final solutions are highly dependent upon initial assumptions for the ECDs, even when small numbers are localized (Uutela *et al* 1998). Another disadvantage of the ECD model is that it has a large possibility of being fitted outside the grey matter of the cerebral cortex, because conventional ECD models have not considered any anatomical information on the brain. In contrast to the ECD model, the distributed source model assumes a lot of current dipoles scattered in limited source spaces (usually on tessellated cerebral cortex) and orientations and/or strengths of the dipoles are then determined using linear or nonlinear estimation methods (Fuchs *et al* 1999, Dale and Sereno 1993, Im *et al* 2003, Bonmassar *et al* 2001). The distributed source approach does not require preliminary information on the numbers and initial locations of brain activations, which allows inexperienced users to localize MEG and EEG sources more easily. Moreover, the distributed source model is physiologically more plausible than the ECD model, because it restricts the possible source space based on the real brain anatomy. When the distributed source model is applied to focal source localizations, we usually regard local peak positions of the source distributions as the locations of the brain sources (Baillet *et al* 2001b, Jerbi *et al* 2002). However, the authors found that the peak positions of the reconstructed sources were sometimes wrongly localized, far from actual sources. We believe that the error stems from the following two reasons. (1) The distributed source model usually uses a spontaneous time slice to solve the inverse problem. Hence, large noises at some time slices may degrade localization accuracy. (2) The distributed source model assumes a large number of dipole sources over several thousands. Therefore, large crosstalk between adjacent dipoles distorts reconstructed source distribution (Liu *et al* 1998).

In this paper, a novel approach to enhance the localization accuracy is proposed. The proposed approach can be classified as a kind of hybrid algorithm, which takes full advantages from both the ECD model and the distributed source model. To solve the problems of the

ECD model, initial regional dipoles are placed at local peak positions of extended sources that are obtained from pre-execution of the distributed source model. The locations of the rotating dipoles are then adjusted on the tessellated cortical surface that was used previously for the distributed source reconstruction. To localize the sources, we proposed a new scheme named the cortical surface scanning algorithm, which scans neighbouring nodes that minimize errors between measured and calculated field quantities.

The proposed anatomically constrained dipole adjust (ANACONDA) approach has many advantages over the conventional models: (1) as the approach assumes small numbers of dipolar sources, crosstalk hardly influences the localization accuracy; (2) as the cortical surface scanning algorithm is a kind of spatio-temporal dipole fit algorithm, it is robust with respect to noise; (3) it requires no additional *a priori* assumptions on the numbers and initial locations of rotating dipoles since it utilizes reconstructed source distributions; (4) as the locations of dipoles are restricted only on the tessellated cortical surface, it is physiologically more plausible than the conventional ECD model that considers no anatomical information.

To verify the advantages listed above, the proposed approach was applied to several case studies. First, it was applied to MEG and EEG forward data simulated with realistic anatomy and real background MEG/EEG signals. Then, it was applied to an MEG experiment (language lexical judgment test) (Fujimaki *et al* 1999, 2002) and an EEG experiment (bilateral epilepsy) (Lin *et al* 2003). From the extensive analyses, it will be shown that the proposed approach can enhance the source localization accuracy considerably, compared to the conventional ones.

2. Methods

2.1. Generalized inverse operator and Wiener regularization

We used a linear estimation approach (Dale and Sereno 1993, Dale *et al* 2000) to reconstruct cortically distributed brain sources. The expression for the inverse operator **W** is

$$\mathbf{W} = \mathbf{R}\mathbf{A}^{\mathrm{T}}(\mathbf{A}\mathbf{R}\mathbf{A}^{\mathrm{T}} + \lambda^2\mathbf{C})^{-1}, \tag{1}$$

where **A** is the lead field matrix which relates sources and sensors, **R** is a source covariance matrix and **C** is a noise covariance matrix. The source distribution can be estimated by multiplying the measured signal at a specific instant **x** by **W**. If we assume that both **R** and **C** are scalar multiples of the identity matrix, this approach becomes identical to minimum norm estimation (Liu *et al* 2002). In this study, the source covariance matrix **R** was assumed to be a diagonal matrix, which means that we ignored relationships between neighbouring sources. The lead field weightings (Gorodnistky *et al* 1995) were imposed on each diagonal entry of **R**. In this study, a pre-stimulus time window was used to calculate **C**. λ^2 is a regularization parameter and was determined systematically using the following equation (Lin *et al* 2004):

$$\lambda^2 = \frac{\text{trace}\,(\mathbf{A}\mathbf{R}\mathbf{A}^T)}{\text{trace}\,(\mathbf{C})\text{SNR}^2}, \tag{2}$$

where trace (.) and SNR represent the sum of diagonal terms and signal-to-noise ratio, respectively.

2.2. Detecting local peak positions of distributed sources

To apply the proposed algorithm, we have to detect local peak positions of distributed sources. To detect local peak positions of distributed sources in an automatic manner, we proposed the following processes.

(1) Local peaks were searched by scanning all source points on a tessellated cortical surface. The local peak is defined as a vertex that has larger current strength than all its neighbouring vertices.
(2) Some vertices whose current strengths were less than a predetermined threshold were excluded from candidates of the local peaks. The threshold was determined based on the signal-to-noise ratio (SNR). The SNR was calculated by integrating signal and noise powers with respect to time. The pre-stimulus time window which includes background MEG/EEG signals was regarded as the noise window.
(3) A local peak that has the largest value was selected among the candidates. Some local peaks that are located close to the selected one were excluded from the candidate set. The critical distance to discriminate sources was determined using a statistical method (Fujimaki *et al* 2002). The critical distances for 148-channel MEG and 45-channel EEG systems used in this study were set to be 33 mm and 43 mm, respectively.
(4) The process (3) was repeated until no candidates were left.

2.3. Cortical surface scanning algorithm

After reconstructing distributed sources, we applied an anatomically constrained dipole fit algorithm named cortical surface scanning. Detailed processes are as follows.

(1) Place rotating dipoles at cortical vertices nearest to local peak positions of the reconstructed source distribution. The local peak positions were found by the automated detection process introduced in the previous section.
(2) Estimate moment vectors of the rotating dipoles using truncated singular value decomposition (tSVD) and calculate an error function. The error function was defined as a Frobenius norm of the difference between measured and calculated field for the considered signal window (Mosher *et al* 1992).
(3) Calculate sensitivity for all dipoles. Sensitivity of a dipole is defined as the maximal change of the error function when a dipole point is moved to its neighbouring vertices. When all possible movements of a dipole do not reduce the error function any more, the value of the sensitivity is set to be 0. To determine the neighbouring vertices, we first determined a constant radius. Then, vertices of which the Euclidean distance from a specified vertex does not exceed the predetermined radius were assigned as the neighbouring vertices of the specified one. The number of neighbouring vertices was then determined considering computational time and the total number of cortical vertices, by adjusting the radius. We assumed about 100 neighbouring vertices for each dipole according to experience (the number of cortical vertices was about 10 000).
(4) A dipole with largest sensitivity is moved to its best neighbouring vertex that reduces the error function most.
(5) Steps (2)–(4) are repeated until sensitivities of all dipoles become 0.

The proposed algorithm can be regarded as a kind of deterministic algorithm. Therefore, it can deal with several brain sources independently and robustly. Moreover, as we can see from the process (2), the algorithm is based on spatio-temporal dipole fit. Thus, it is very robust to noise components, especially to white Gaussian noise. Contrary to conventional dipole fit algorithms, the proposed one assumes initial locations and numbers of the regional sources based on the results of pre-executed distributed source reconstruction. Therefore, the algorithm has a small risk to be trapped in local minima. To verify its usefulness and validness, it was applied to various simulations and experiments.

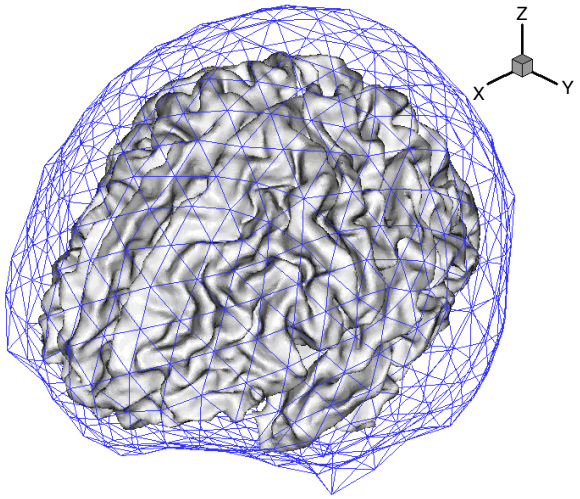

Figure 1. Anatomical data used for MEG forward/inverse calculations—tessellated cortical surface and boundary element meshes (inner skull boundary). Note that the cortical surface was not included in the boundary element analysis.

3. Validation by simulation studies

Neuroelectromagnetic inverse problems are very hard to verify by *in vivo* experiments because exact source locations inside the real human brain cannot be estimated *a priori*. For this reason, artificially constructed forward data are widely used to validate MEG and EEG inverse algorithms (Kincses *et al* 1999). Hence, we first applied the proposed technique to artificially constructed MEG and EEG data.

3.1. Constructing artificial MEG data

We assumed realistic conditions obtained from a practical measurement that will be used again in the next section. The sensor layout used for the simulation was a 148-channel whole-head MEG system (Magnes 2500 WH; Biomagnetic Technologies, Inc). To utilize anatomical information, the interface between white and grey matters was extracted from MRI T1 images ($256 \times 256 \times 200$, voxel size for each direction: 1 mm) and tessellated into 510 267 triangular elements including 255 329 vertices. To extract and tessellate the cortical surface, we applied *BrainSuite* developed in the University of Southern California, CA, USA (Shattuck and Leahy 2002). In this paper, the boundary element method (BEM) was applied for the forward calculation of magnetic field. It has been frequently reported that just considering the inner skull boundary is sufficient for the MEG forward calculations (Meijs *et al* 1988, Hämäläinen and Sarvas 1989). The boundary surface used for the BEM was composed of 1016 elements and 510 nodes. Figure 1 demonstrates the tessellated cortical surface and the boundary element meshes.

Nowadays, for the forward calculations, generating artificial activation patches on a brain cortical surface has been popularized instead of activating some point sources (Im *et al* 2003). To generate cortical patches and construct a forward data set, the concept of virtual area was adopted (Chupin *et al* 2002). A virtual area was assigned to each vertex as a third of the area of all triangles meeting at a vertex. This assumption is valid because the total virtual area

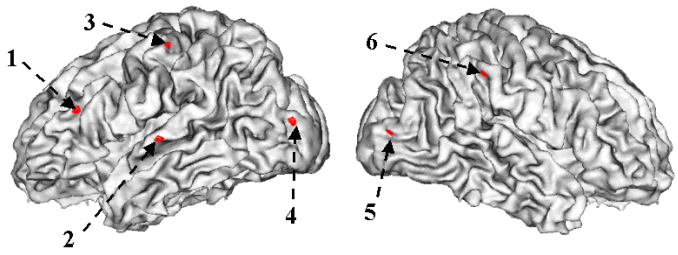

Figure 2. Locations of six sources assumed to simulate a realistic MEG signal.

remains equal to the actual area of the full tessellation. Then, the cortical patch was generated using the following process: (1) a point is selected as a seed of an activation patch area. (2) The patch area is extended by including neighbouring vertices around the patch. (3) If the total virtual area of the cortical patch exceeds an aimed surface area, the extension of the activation patch is terminated.

Figure 2 shows six small activation patches, of which virtual areas were assumed to be approximately 10 mm^2. Source intensity patterns I of the six sources with respect to time t were assumed as follows.

Source 1 and source 4:

$$I = -0.6 \times 10^{-4}(t - 100)^2 + 0.6 \qquad (0\,\text{ms} \leqslant t < 200\,\text{ms})$$
$$= 0 \qquad (200\,\text{ms} \leqslant t < 400\,\text{ms}).$$

Source 3 and source 5:

$$I = 0 \qquad (0\,\text{ms} \leqslant t < 100\,\text{ms})$$
$$= -0.6 \times 10^{-4}(t - 200)^2 + 0.6 \qquad (100\,\text{ms} \leqslant t < 300\,\text{ms})$$
$$= 0 \qquad (300\,\text{ms} \leqslant t < 400\,\text{ms}).$$

Source 2 and source 6:

$$I = 0 \qquad (0\,\text{ms} \leqslant t < 200\,\text{ms})$$
$$= -0.6 \times 10^{-4}(t - 300)^2 + 0.6 \qquad (200\,\text{ms} \leqslant t < 400\,\text{ms}).$$

After the forward calculation of magnetic field assuming a 670 Hz sampling rate, we added real background MEG signals, which were obtained from the pre-stimulus period of a practical experiment. The original signal without background noise was scaled in order for signal-to-noise ratio to be approximately 10. Figure 3 shows the finally constructed signal patterns for 148 channels with respect to simulated time.

3.2. Constructing artificial EEG data

We also assumed realistic conditions to construct artificial EEG data. All these preprocessed data were also applied to the experimental studies that will be presented in the next section. We used 45 electrodes which were attached on a subject's scalp according to the extended 10–20 electrode system (Nuwer *et al* 1998). The MRI T1 image was obtained from a 1.5 T commercial MRI machine. 641 195 elements and 321 698 vertices were generated using *BrainSuite* as in the MEG study. In contrast to the MEG forward calculation, full head structures should be taken into account for the EEG forward calculations (Liu *et al* 2002). In this dissertation, a three-layer model, consisting of inner and outer skull boundary and scalp surface, was used. Figure 4 shows the boundary elements co-registered with the tessellated cortical surface.

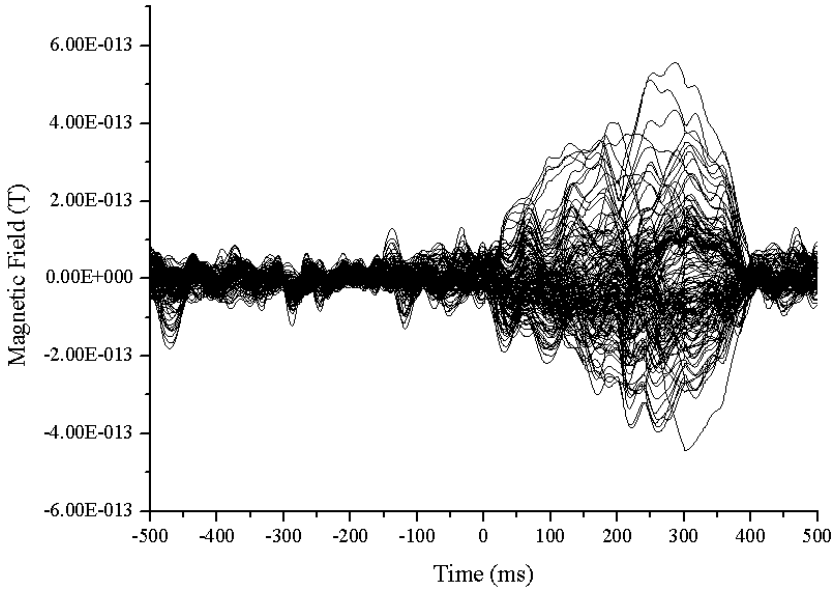

Figure 3. Simulated MEG signals with real background MEG signal (SNR = 10).

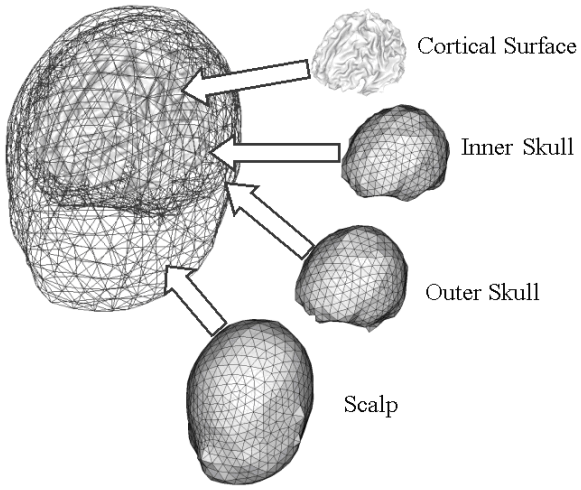

Figure 4. Boundary element model for EEG forward calculations. 3260 elements and 1836 nodes were generated. Note that the cortical surface meshes were not included in the EEG forward calculation. They were used only for positioning dipole sources.

Then, considering relatively smaller number of sensors in EEG, four activation patches, of which virtual areas were assumed to be approximately 10 mm^2, were generated as depicted in figure 5. The source intensity patterns I of the four sources with respect to time t were assumed as follows.

Source 1 and source 3:

$$I = -0.6 \times 10^{-4}(t - 100)^2 + 0.6 \qquad (0\,\text{ms} \leqslant t < 200\,\text{ms})$$
$$= 0 \qquad (200\,\text{ms} \leqslant t < 400\,\text{ms}).$$

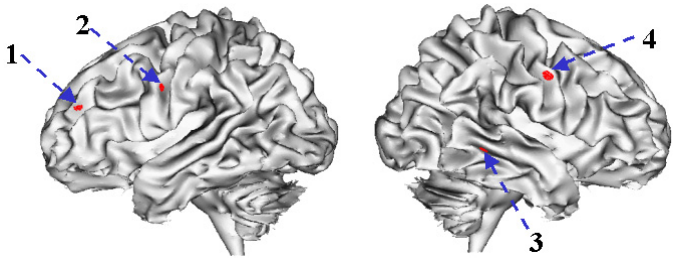

Figure 5. Locations of four sources assumed to simulate a realistic EEG signal.

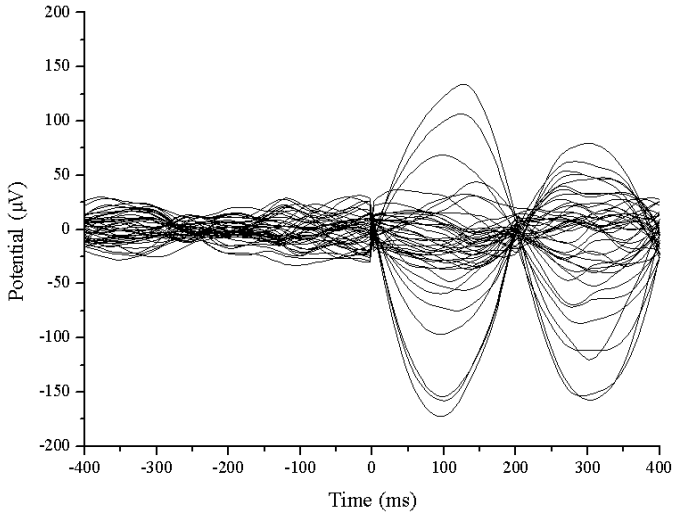

Figure 6. Simulated EEG signals with real background EEG signal (SNR = 10).

Source 2 and source 4:

$$I = 0 \qquad (0\,\text{ms} \leqslant t < 200\,\text{ms})$$
$$= -0.6 \times 10^{-4}(t - 300)^2 + 0.6 \qquad (200\,\text{ms} \leqslant t < 400\,\text{ms}).$$

After calculating the electric potential at the 45-channel electrodes assuming 200 Hz sampling rate, we added real background EEG signals, which were obtained from the pre-stimulus period of a practical EEG experiment. The original signal without any noise was scaled in order for the signal-to-noise ratio to be approximately 10. Figure 6 shows the artificial EEG signals with respect to time.

3.3. Application to MEG data

We first reconstructed source distributions at 100 ms, 200 ms and 300 ms of the artificial MEG data presented in figure 3. For imposing an anatomical constraint, the tessellated cortical surface was sampled to be 10 204 dipole locations. In the simulation, we did not constrain the orientations of the dipoles from a consideration that there was much ambiguity introduced by a geometrical modelling error[4]. Figures 7(a)–(c) show the reconstructed source

[4] The geometrical modelling error represents that some cortical areas were not properly segmented. The segmented cortical surface used in this paper had the same problem. In particular, the sulci-gyri structures around the occipital

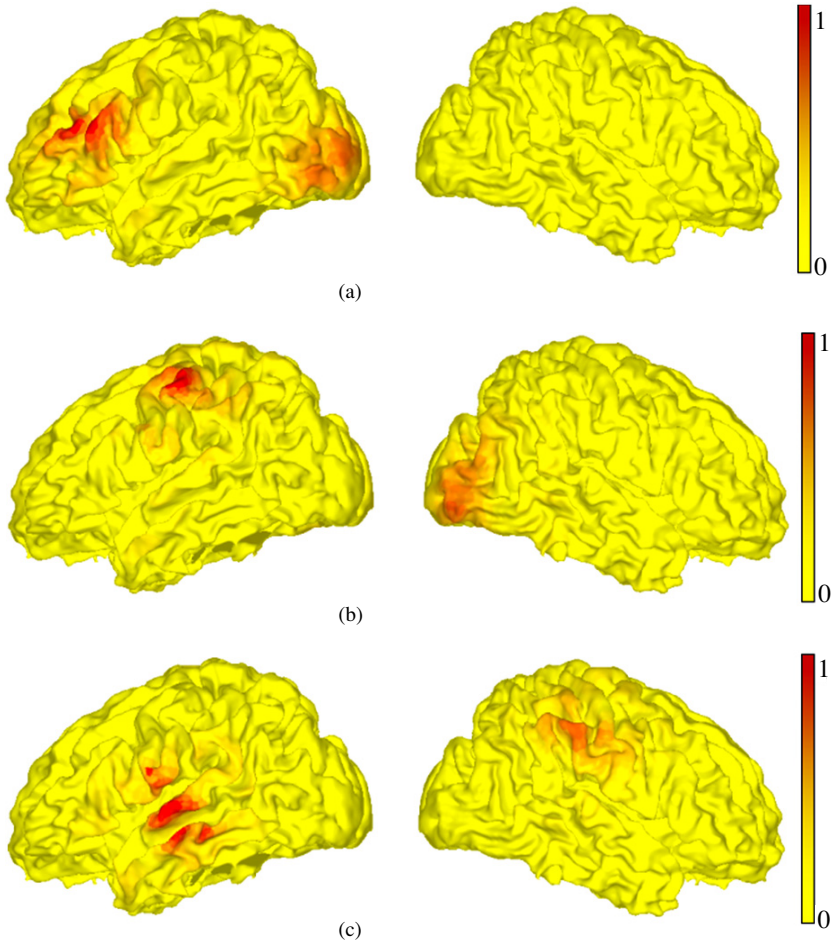

Figure 7. Normalized current dipole power at (a) 100 ms, (b) 200 ms and (c) 300 ms—MEG simulation. The values were normalized with respect to maximum power of each time.

distributions. Throughout this paper, noise normalized current dipole power (sum of squared dipole component strengths) was used for visualization purposes (Dale *et al* 2000).

After the reconstruction, we placed some rotating dipoles at local peak positions and applied the cortical surface scanning algorithm. The time window considered for the spatio-temporal dipole fit was −20 ms to 20 ms with respect to the central times. Table 1 presents exact locations of six activation patches (centre of gravity), initial locations of regional sources (detected local peak positions), positions of regional sources after applying the cortical surface scanning algorithm, and localization errors. In figure 8, the positions of exact activations, local peaks and regional sources are visualized on the tessellated cortical surface. We can see from the table and the figure that the localization accuracy was considerably enhanced by the introduction of the proposed approach.

lobe were not properly segmented because of inhomogeneity of MRI images and other technical problems. That is why we did not constrain the source orientations.

Table 1. Comparison of localization accuracy between distributed source reconstruction and cortical surface scanning algorithm—results of simulations for realistic MEG forward data (figure 3). 'Peak' in parentheses represents local peak positions of distributed sources and 'scanning' means locations of regional sources after applying the cortical surface scanning algorithm.

Source number (conditions)	x (mm)	y (mm)	z (mm)	Error (mm)
1 (exact)	55.59	42.70	68.31	–
1 (peak)	53.02	52.16	64.95	10.36
1 (scanning)	58.44	41.58	70.14	3.57
2 (exact)	17.22	65.40	47.96	–
2 (peak)	16.18	67.74	51.43	4.31
2 (scanning)	15.36	65.85	48.74	2.07
3 (exact)	10.53	51.66	97.81	–
3 (peak)	13.09	47.41	102.08	6.55
3 (scanning)	6.94	50.76	98.09	3.71
4 (exact)	−54.90	32.33	55.29	–
4 (peak)	−63.25	33.86	51.27	9.39
4 (scanning)	−54.76	32.87	57.00	1.80
5 (exact)	−57.83	−34.14	54.45	–
5 (peak)	−62.62	−36.94	41.94	13.69
5 (scanning)	−56.30	−31.62	58.43	4.95
6 (exact)	−8.99	−52.73	87.74	–
6 (peak)	−2.25	−57.25	83.82	9.01
6 (scanning)	−4.49	−55.60	86.02	5.61

3.4. Application to EEG data

Then, we applied the linear inverse approach to the artificial EEG data. As in the MEG case, 10 723 vertices were sampled from the original 321 698 vertices. Figures 9(a) and (b) show the reconstructed source distributions at 100 ms and 200 ms, respectively.

After the distributed source reconstruction, the proposed algorithm was applied in the same manner as the MEG case. Initial regional sources were placed at local peak positions of the reconstructed distribution. Table 2 presents exact locations of four activation patches (centre of gravity), initial locations of regional sources (local peak positions), positions of regional sources after applying the cortical surface scanning algorithm, and localization errors. In figure 10, the positions of exact activations, local peaks and regional sources are visualized on the tessellated cortical surface. From the results, we can observe that the localization accuracy was also enhanced greatly by the introduction of the cortical surface scanning algorithm.

3.5. Extended simulations for multiple activations

In the previous MEG and EEG simulations, only two sources were activated simultaneously. In this section, the cortical surface scanning algorithm was applied to more complex data simulated with more than four simultaneous activations. In both MEG and EEG simulations, the positions of exact source patches were the same as those in previous simulations (see figures 2, 5). Instead, all the sources were activated simultaneously with the following source intensity pattern:

$$I = -0.6 \times 10^{-4}(t - 100)^2 + 0.6 \qquad (0\,\text{ms} \leqslant t < 200\,\text{ms})$$
$$= 0 \qquad (200\,\text{ms} \leqslant t < 400\,\text{ms}).$$

After reconstructing the distributed sources, the cortical surface scanning algorithm was applied. After 15 iterations in MEG and 12 iterations in EEG, all the MEG and EEG regional

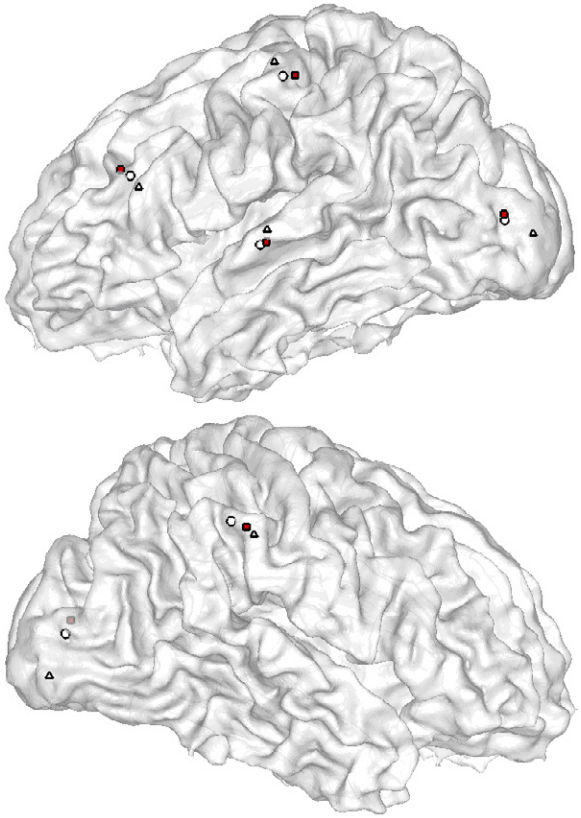

Figure 8. Comparisons of MEG source locations before and after applying the cortical surface scanning algorithm: circles—exact locations, triangles—initial locations, coloured rectangles—final locations.

sources were converged. Table 3 (figure 11) and table 4 (figure 12) show the locations of exact activation patches, initial local peaks and final regional sources for MEG and EEG, respectively. In spite of the fact that the simulation conditions were more complex than those of the previous simulations, all regional sources were successfully localized by the cortical surface scanning algorithm with small localization errors comparable to the previous results. We can see from the results that the proposed algorithm is very robust even when the number of simultaneous sources exceeds four. In practical experiments, the number of simultaneous activations at a certain time slice often exceeds three or four (Fujimaki *et al* 2002). In such cases, it is extremely difficult to localize the multiple sources using the conventional ECD method without preliminary information on the numbers and initial locations of the ECDs. The authors expect that the cortical surface scanning algorithm can overcome the difficulty because the algorithm starts from good initial guesses on the numbers and locations of the regional sources.

4. Applications to practical measurements

The ANACONDA approach was applied to practical MEG and EEG measurements. In the case of such practical measurements, it is very difficult to verify the localization accuracy

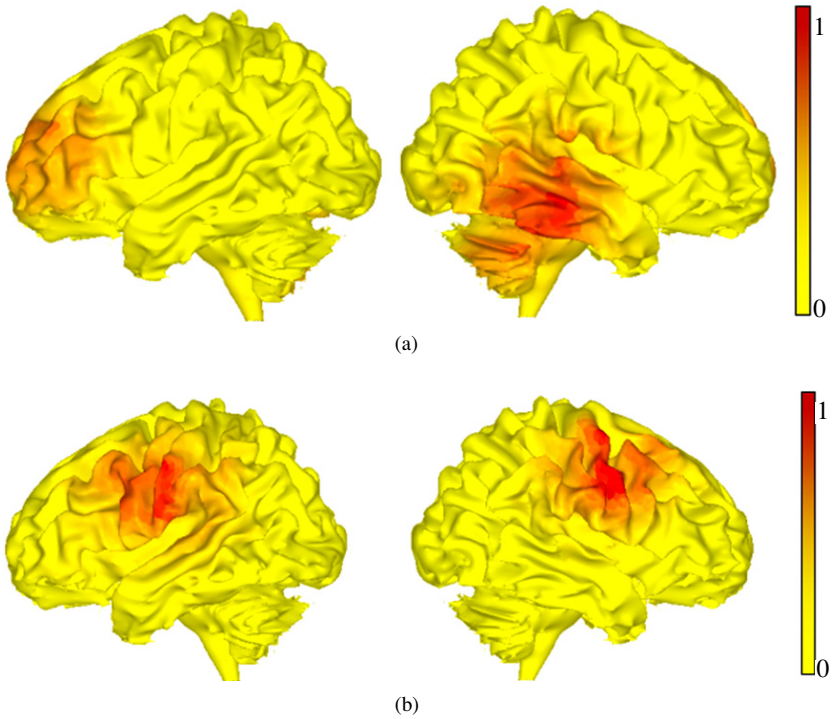

Figure 9. Normalized current dipole power at (a) 100 ms and (b) 200 ms—EEG simulation. The values were normalized with respect to maximum power of each time.

Table 2. Comparison of localization accuracy between distributed source reconstruction and cortical surface scanning algorithm—results of simulations for realistic EEG forward data (figure 6). 'Peak' in parentheses represents local peak positions of distributed sources and 'scanning' means locations of regional sources after applying the cortical surface scanning algorithm.

Source number (conditions)	x (mm)	y (mm)	z (mm)	Error (mm)
1 (exact)	67.42	26.89	66.84	–
1 (peak)	68.85	29.24	70.10	4.27
1 (scanning)	67.77	27.79	67.96	1.48
2 (exact)	23.28	48.37	77.86	–
2 (peak)	16.53	57.07	70.92	13.02
2 (scanning)	18.41	50.13	74.57	6.14
3 (exact)	12.78	−65.21	43.65	–
3 (peak)	−1.41	−67.11	37.86	15.44
3 (scanning)	10.24	−61.11	44.54	4.90
4 (exact)	21.68	−55.36	82.35	–
4 (peak)	18.62	−46.70	102.15	21.83
4 (scanning)	17.50	−54.68	87.65	6.78

directly. Therefore, a famous concept called goodness of fit (GOF, the squared sum of the signal explained by the model divided by the squared sum of the total signal) (de Munck *et al* 2001, Chitoku *et al* 2003, Yoshinaga *et al* 2005, Uutela *et al* 1998) was used for these verification studies.

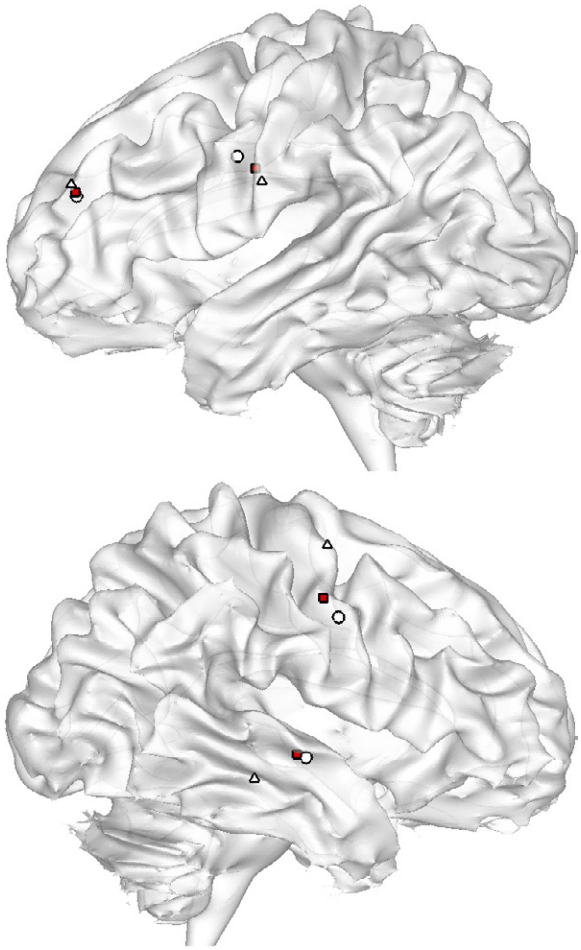

Figure 10. Comparisons of EEG source locations before and after applying the cortical surface scanning algorithm: circles—exact locations, triangles—initial locations, coloured rectangles—final locations.

4.1. Application to an early visual response—an MEG study

A problem considered in this MEG study was a part of a language lexical judgment test (Fujimaki *et al* 1999). Several strings of three characters were visually presented to a right-handed subject. The set of strings was composed of Japanese katakana strings (meaningful nouns) and meaningless pseudo-character strings. The subject answered whether the strings were meaningful or not, by pressing one of two buttons with his left index and middle fingers. The visual stimuli were presented below a square (a fixation mark) every 2 s with a duration of 1 s. The luminance was 15 cd m^{-2} for the stimulus and 0.5 cd m^{-2} for the background, and the visual angle was 1.3° for one character and 0.3° for the fixation mark. A 148-channel whole head magnetometer system was used to record the magnetic field, which was already used in the previous forward simulations. The data were averaged over 200 epochs (pre-trigger period: 500 ms, post-trigger period: 1200 ms) and were filtered with a bandpass of 0.3–40 Hz. Figure 13 shows the measured MEG waveform. In this study, only the earliest visual response

Table 3. Comparison of localization accuracy between distributed source reconstruction and cortical surface scanning algorithm—results of MEG simulations when six patches are activated simultaneously. 'Peak' in parentheses represents local peak positions of distributed sources and 'scanning' means locations of regional sources after applying the cortical surface scanning algorithm.

Source number (conditions)	x (mm)	y (mm)	z (mm)	Error (mm)
1 (exact)	55.59	42.70	68.31	–
1 (peak)	61.23	46.23	65.41	7.26
1 (scanning)	61.23	39.52	70.26	6.76
2 (exact)	17.22	65.40	47.96	–
2 (peak)	22.09	65.99	45.90	5.32
2 (scanning)	15.36	65.85	48.75	2.07
3 (exact)	10.53	51.66	97.81	–
3 (peak)	11.70	53.21	97.63	1.95
3 (scanning)	10.63	51.44	98.77	0.99
4 (exact)	−54.90	32.33	55.29	–
4 (peak)	−62.79	32.21	56.44	7.97
4 (scanning)	−52.38	33.94	59.43	5.11
5 (exact)	−57.83	−34.14	54.45	–
5 (peak)	−62.62	−36.94	41.94	13.69
5 (scanning)	−59.60	−32.34	61.45	7.44
6 (exact)	−8.99	−52.73	87.74	–
6 (peak)	−3.59	−55.23	88.60	6.01
6 (scanning)	−3.94	−51.68	87.91	5.16

Table 4. Comparison of localization accuracy between distributed source reconstruction and cortical surface scanning algorithm—results of EEG simulations when four patches are activated simultaneously. 'Peak' in parentheses represents local peak positions of distributed sources and 'scanning' means locations of regional sources after applying the cortical surface scanning algorithm.

Source number (conditions)	x (mm)	y (mm)	z (mm)	Error (mm)
1 (exact)	67.42	26.89	66.84	–
1 (peak)	67.17	28.35	71.19	4.59
1 (scanning)	67.79	28.10	68.23	1.88
2 (exact)	23.28	48.37	77.86	–
2 (peak)	13.90	52.39	87.29	13.89
2 (scanning)	21.03	45.04	72.11	7.02
3 (exact)	12.78	−65.21	43.65	–
3 (peak)	−1.18	−66.85	38.11	15.11
3 (scanning)	11.15	−66.83	40.90	3.58
4 (exact)	21.68	−55.36	82.35	–
4 (peak)	18.92	−46.42	102.00	21.76
4 (scanning)	20.20	−52.32	88.28	6.83

(80 ms) was investigated, because this kind of simple response is relatively more focalized compared to other complex responses.

Figure 14 shows the magnetic field map on a sensor plane and reconstructed source distributions[5] at 80 ms. We can see from the results that the earliest visual activations were

[5] All the conditions used for the calculations were exactly the same as those of the previous forward simulations, such as anatomical constraints, sensor positions and BEM meshes. Pre-stimulus time (−500–0 ms) was regarded as the noise window, which was used to construct noise covariance matrix **C**.

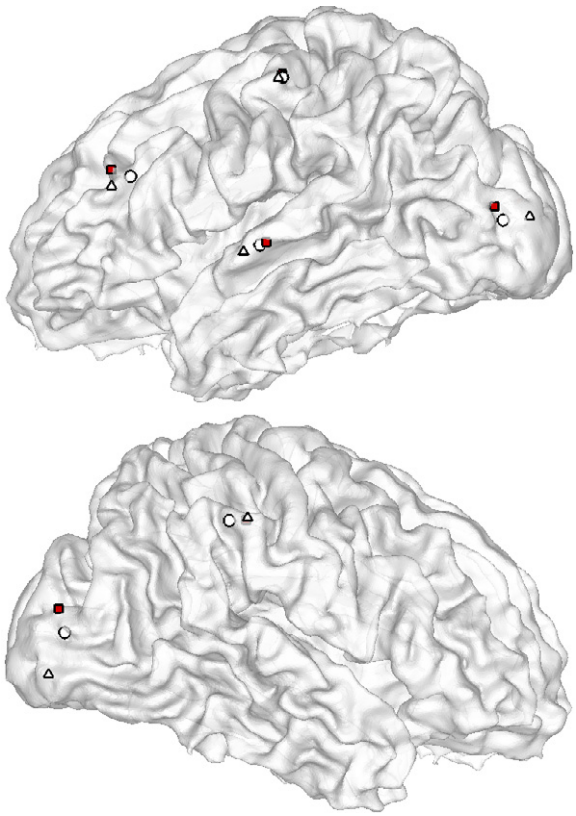

Figure 11. Comparisons of MEG source locations before and after applying the cortical surface scanning algorithm, when six patches were activated simultaneously (circles—exact locations, triangles—initial locations, coloured rectangles—final locations).

observed as expected. After applying the local peak detection processes, three regional sources were placed at the local peak positions. Positions of the regional sources were then adjusted using the cortical surface scanning algorithm. Figure 15 presents the initial and final positions of the regional sources, where slight changes were observed. Figure 16 shows the variation of GOF with respect to the number of iterations, from which we can see that the source localization accuracy was enhanced by the introduction of the anatomically constrained dipole adjustment processes. Actually, if the number of dipoles increases, the GOF value should increase as well (Uutela *et al* 1998). In this study, the number of dipoles was fixed throughout the iteration and only location parameters of dipoles were changed. In such a case, the increased GOF implies that the new positions can express the electromagnetic quantities measured outside the head more reasonably than the initial positions.

For comparison, we applied the conventional ECD approach that does not consider anatomical information to the same data set. We used the peak positions of the distributed sources as the initial locations of the ECDs, but did not constrain their locations on the cortical surface during the iteration. A spatio-temporal objective function was used as in the cortical surface scanning method and a standard simplex search was adopted as an optimization algorithm, which has been extensively used for the dipole localization (Cuffin 1995, Finke *et al* 2003). The iteration was terminated when the Euclidean distance between simplex solutions reduced below 1 mm. As expected, some ECDs were localized far from the tessellated cortical

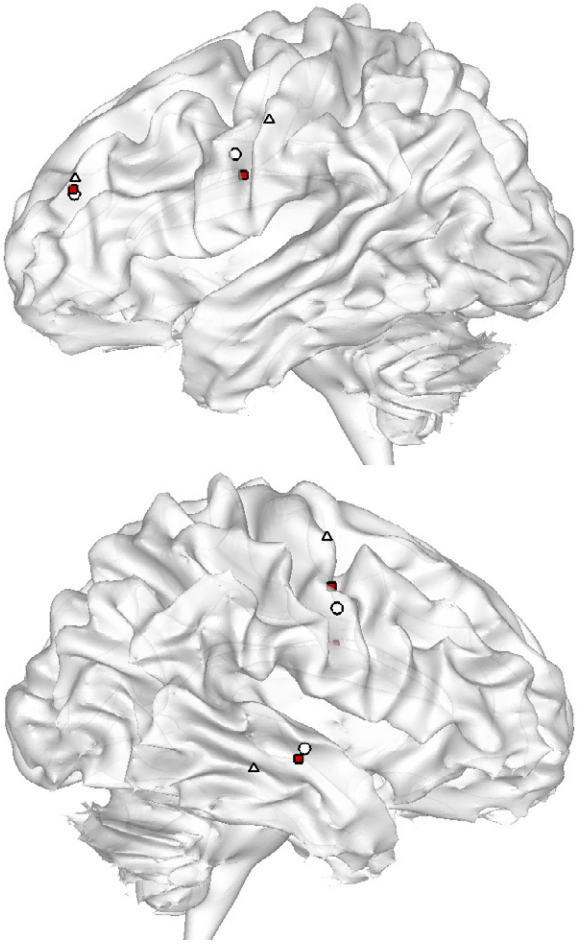

Figure 12. Comparisons of EEG source locations before and after applying the cortical surface scanning algorithm, when four patches were activated simultaneously (circles—exact locations, triangles—initial locations, coloured rectangles—final locations).

surface. To quantify the degree of the mislocalization, we calculated the minimal distance between the localized dipole locations and the cortical surface. Note that the developments of medical image processing techniques and high resolution structural MRI enabled us to get a high resolution cortical surface with sub-millimeter modelling errors (Dale *et al* 1999, Fischl and Dale 2000), which is even lower than the MRI voxel resolutions. The evaluated distances were 7.43 mm (left superior source), 3.23 mm (left inferior source) and 5.21 mm (right source). Therefore, it can be seen that some ECDs were localized outside the cerebral cortex even when the thickness of grey matter (generally 4 mm, see Fischl and Dale (2000)) is considered.

4.2. Application to bilaterally synchronous discharge in benign Rolandic epilepsy of childhood—an EEG study

Benign Rolandic epilepsy of childhood (BREC) is a common primary partial epilepsy syndrome, which usually appears in children under the age of 15 (Lin *et al* 2003). The interictal

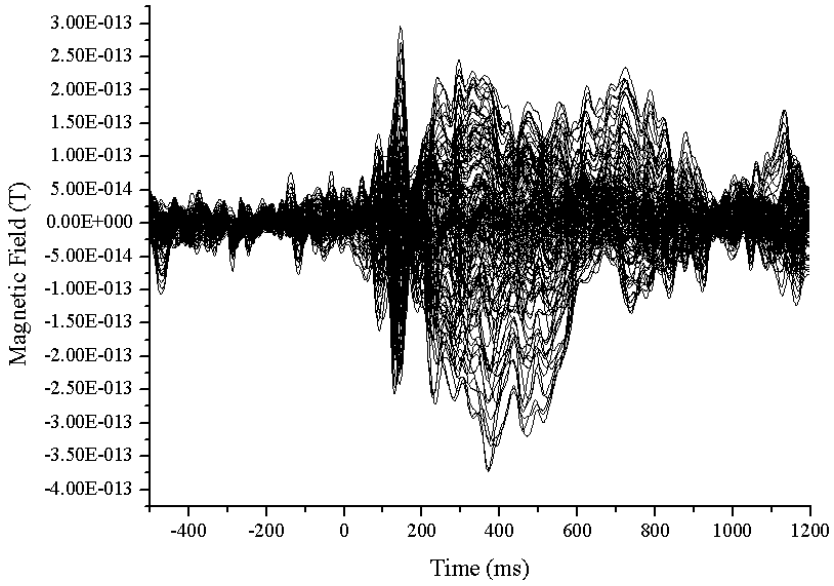

Figure 13. MEG waveform of a subject measured with 148-channel magnetometers. Over 200 epochs of data were averaged and filtered with a bandpass of 0.3–40 Hz.

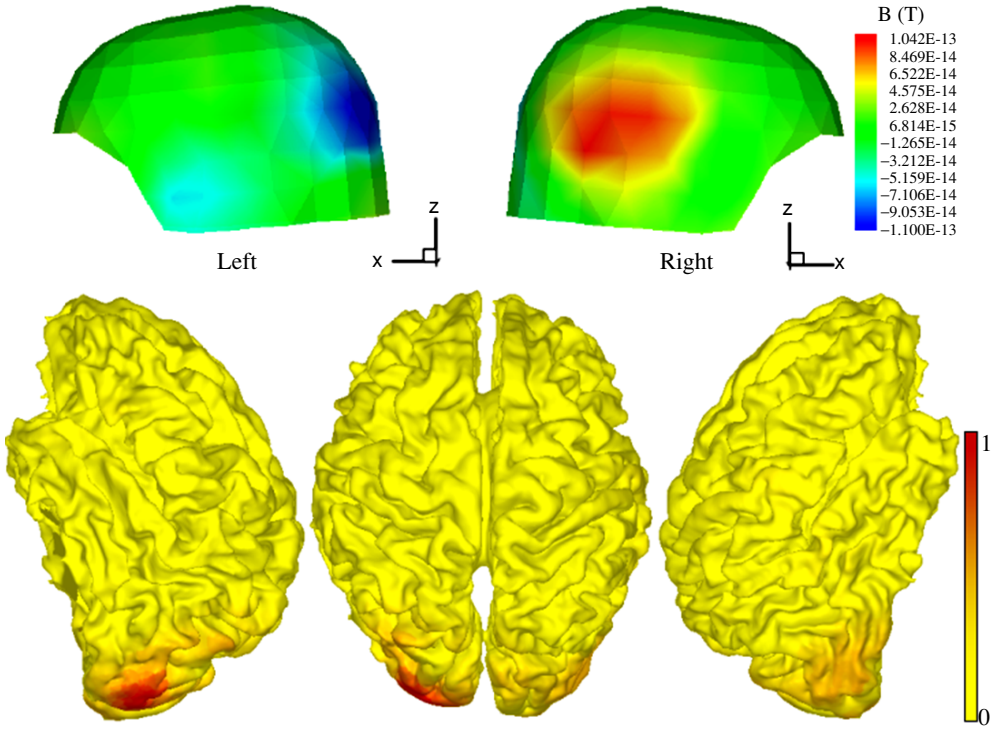

Figure 14. Magnetic field map on a sensor plane and reconstructed source distribution at 80 ms. The value of the contour intensity was normalized with respect to the maximum power.

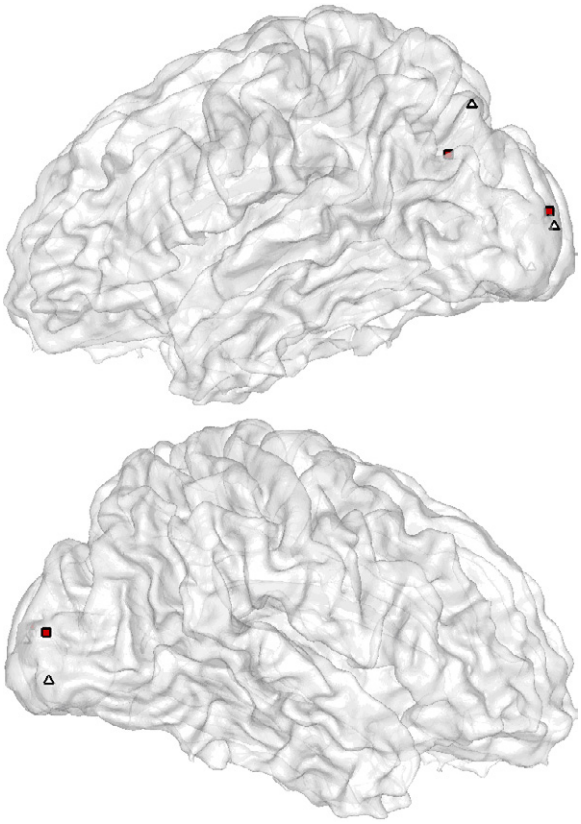

Figure 15. Comparisons of source locations ($t = 80$ ms) before and after applying the cortical surface scanning algorithm (triangles—initial locations, coloured rectangles—final locations).

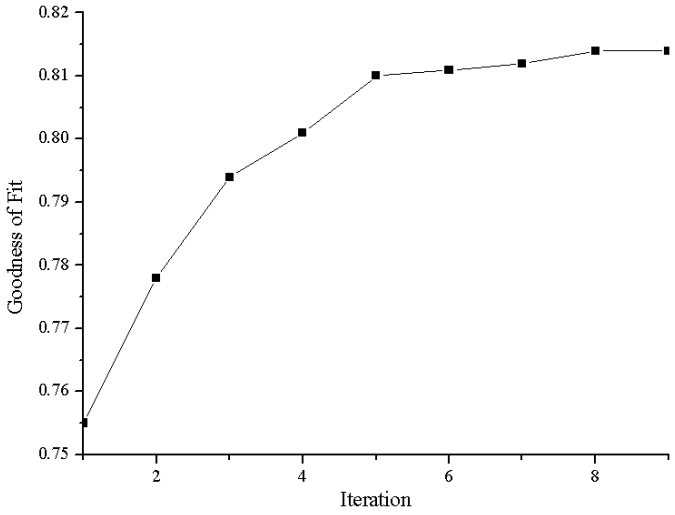

Figure 16. Variation of GOF with respect to iteration. Locations of three dipoles were fitted after eight iterations.

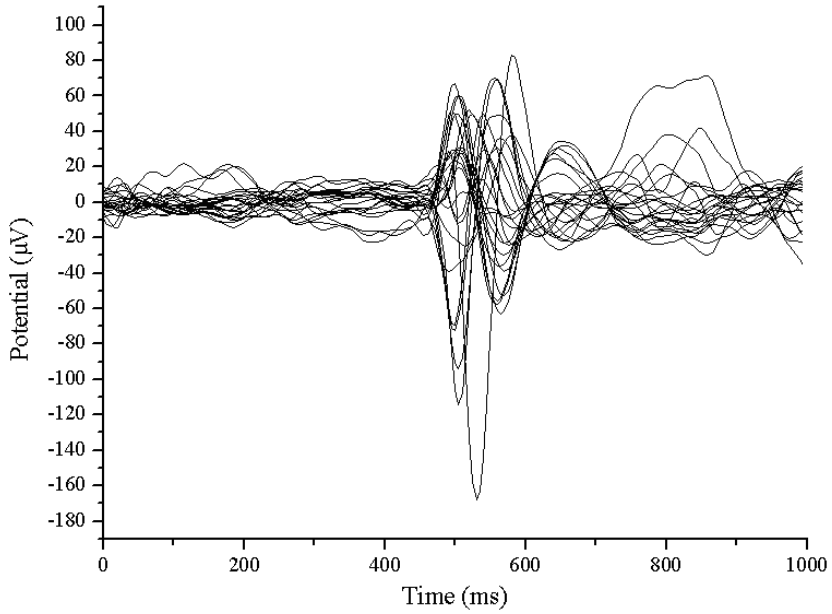

Figure 17. Averaged interictal epileptic spike measured by scalp EEG.

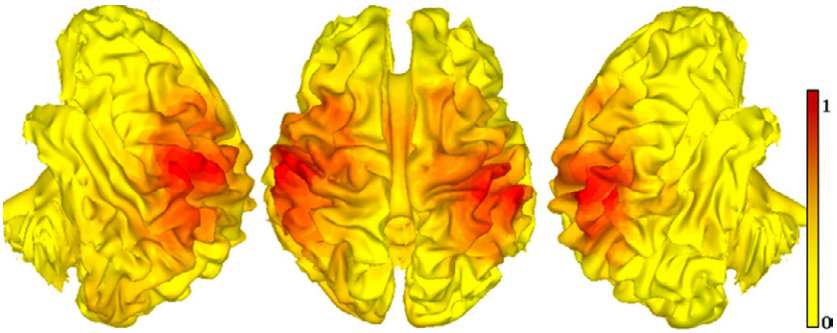

Figure 18. Source distribution reconstructed at 500 ms. The contour levels were normalized with respect to the maximum power.

spike waveform of a child whose spike can be viewed as a bilaterally synchronous discharge (BSD) was measured using the scalp EEG system introduced in the previous section. Figure 17 shows the averaged EEG signals. Then, the EEG source distribution was reconstructed at 500 ms. Figure 18 shows the epileptic source distribution estimated at 500 ms.

After detecting the local peak positions, two regional sources were placed therein. Positions of the regional sources were then adjusted using the cortical surface scanning algorithm. Figure 19 presents the initial and final positions of the regional sources. Figure 20 shows the variation of GOF with respect to iteration, from which we can see that the localization accuracy was considerably enhanced by the proposed algorithm.

Then, we applied the conventional ECD approach that does not consider any anatomical information in the same manner as the previous MEG analysis. The minimal distances between

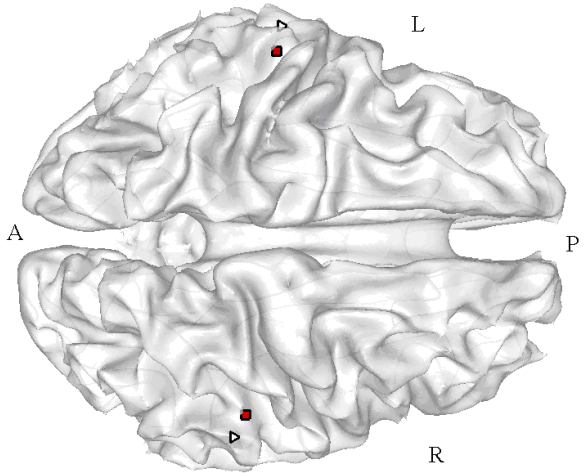

Figure 19. Comparisons of source locations ($t = 500$ ms) before and after applying the cortical surface scanning algorithm (triangles—initial locations, coloured rectangles—final locations).

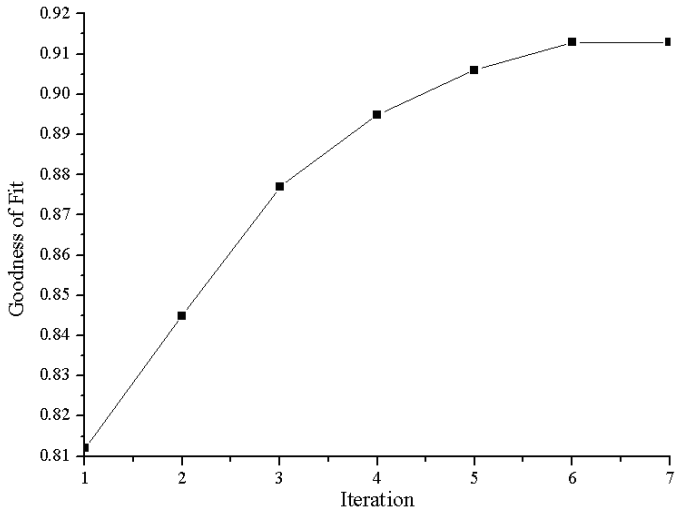

Figure 20. Variation of GOF with respect to iteration. Locations of two dipoles were fitted after seven iterations.

the localized position and the cortical surface were 7.95 mm (left source) and 3.12 mm (right source), from which it can be seen that some ECDs were localized outside the cerebral cortex as in the MEG case.

5. Conclusions

In this paper, a novel approach to enhancing localization accuracy of MEG and EEG focal sources was proposed, which can overcome several disadvantages of two conventional approaches, the equivalent current dipole (ECD) model and the distributed source model.

The novel approach proposed in this paper assumes anatomically constrained spatio-temporal dipoles, initial positions of which are estimated from local peak positions of distributed sources obtained from a pre-execution of distributed source reconstruction. The positions of the regional sources are then adjusted on a tessellated cortical surface using a novel updating scheme named the cortical surface scanning algorithm.

The proposed approach was applied to various realistic simulations and practical experiments. For the MEG and EEG simulations, realistic conditions that were obtained from practical experiments were assumed and real background MEG/EEG signals in the pre-stimulus time window were added to the forward data. For the forward calculations, the boundary element method was applied. From the forward simulations, it was shown that the proposed approach could enhance source localization accuracy compared to the conventional distributed source model. Then, the authors applied the proposed approach to MEG and EEG experiments. To verify and compare the results, a goodness of fit (GOF) was applied. From the analyses, we could also observe that the cortical surface scanning algorithm could considerably enhance GOF of localizations, compared to the distributed source model.

In summary, the proposed approach has shown the following advantages and characteristics: (1) as the cortical surface scanning algorithm is a kind of spatio-temporal dipole fit algorithm, it is robust with respect to noise. Moreover, as the approach assumes only small numbers of regional sources, crosstalk between adjacent sources does not affect the localization accuracy. Those are why the ANACONDA approach yielded more accurate localization results than the distributed source model. (2) It requires no preliminary assumptions on the numbers and initial locations of rotating dipoles since it utilizes reconstructed distributed sources; (3) as the locations of dipoles are restricted only on the tessellated cortical surface, it is physiologically more plausible than the conventional ECD model that considers no anatomical information; (4) when applying the proposed approach, multiple sources can be localized robustly because the cortical surface scanning algorithm starts from good initial guesses on the numbers and locations of the sources.

It is evident that the proposed approach is more suitable for focal source localization problems such as sensory and epileptic source localizations, compared to other applications such as perception, language, memory and so on, for which rough distributions of MEG and EEG sources are often sufficient. In such focal source applications, to reduce localization errors is a very crucial problem because it is often related to a subject's life. Unfortunately, spatial configurations of MEG and EEG sensors are limited on the order of a few hundreds and enhancement of the localization accuracy by the use of more sensors has been nearly saturated. Hence, it is expected that the proposed approach will become a promising alternative.

In future, more studies should be continued. As processes to scan neighbouring vertices require considerable computation time, developments of more efficient scanning techniques will enhance the overall efficiency of the proposed approach. In addition, to get more generality, the proposed approach should be applied to more problems. Epilepsy is thought to be a very good application because some epileptic source locations can be assured after surgeries.

Acknowledgments

This work was supported by a Korea Research Foundation Grant funded by the Korean Government (MOEHRD, Basic Research Promotion Fund) (M01-2005-000-10132-0). The authors are grateful to Dr Ki-Young Jung (MD in Department of Neurology, Samsung Medical Center, Korea) for providing us with epilepsy data.

References

Baillet S, Mosher J C and Leahy R M 2001a Electromagnetic brain mapping *IEEE Signal Process. Mag.* **18** (Nov) 14–30

Baillet S, Riera J J, Marin G, Mangin J F, Aubert J and Garnero L 2001b Evaluation of inverse methods and head models for EEG source localization using a human skull phantom *Phys. Med. Biol.* **46** 77–96

Bonmassar G, Schwartz D P, Liu A K, Kwong K K, Dale A M and Belliveau J W 2001 Spatiotemporal brain imaging of visual-evoked activity using interleaved EEG and fMRI recordings *Neuroimage* **13** 1035–43

Chitoku S *et al* 2003 Characteristics of dipoles in clustered individual spikes and averaged spikes *Brain Dev.* **25** 14–21

Chupin M, Baillet S, Okada C, Hasboun D and Garnero L 2002 On the detection of hippocampus activity with MEG *Proc. Conf. on Biomagnetism—BIOMAG 2002*

Cuffin B N 1995 A method for localizing EEG sources in realistic head models *IEEE Trans. Biomed. Eng.* **42** 68–71

Dale A M, Fischl B and Sereno M I 1999 Cortical surface-based analysis: I. Segmentation and surface reconstruction *Neuroimage* **9** 179–94

Dale A M, Liu A K, Fischl B R, Buckner R L, Belliveau J W, Lewine J D and Halgren E 2000 Dynamic statistical parametric mapping: combining fMRI and MEG for high-resolution imaging of cortical activity *Neuron* **26** 55–67

Dale A M and Sereno M I 1993 Improved localization of cortical activity by combining EEG and MEG with MRI surface reconstruction: a linear approach *J. Cognit. Neurosci.* **5** 162–76

de Munck J C, van Dijk B W and Spekreijse H 1988 Mathematical dipoles are adequate to describe realistic generators of human brain activity *IEEE Trans. Biomed. Eng.* **35** 960–6

de Munck J C, de Jongh A and Van Dijk B W 2001 The localization of spontaneous brain activity: an efficient way to analyze large data sets *IEEE Trans. Biomed. Eng.* **48** 1221–8

Ebersole J S 1994 Noninvasive localization of the epileptogenic focus by EEG dipole modeling *Acta Neurol. Scand.* **152** (Suppl.) 20–8

Finke S, Gulrajani R M and Gotman J 2003 Conventional and reciprocal approaches to the inverse dipole localization problem of electroencephalography *IEEE Trans. Biomed. Eng.* **50** 657–66

Fischl B and Dale A M 2000 Measuring the thickness of the human cerebral cortex from magnetic resonance images *Proc. Natl. Acad. Sci. USA* **97** 11050–5

Fuchs M, Wagner M, Kohler T and Wischmann H-A 1999 Linear and nonlinear current density reconstructions *J. Clin. Neurophysiol.* **16** 267–95

Fujimaki N, Hayakawa T, Nielsen M, Knösche T R and Miyauchi S 2002 An fMRI-constrained MEG source analysis with procedures for dividing and grouping activation *Neuroimage* **17** 324–43

Fujimaki N, Miyauchi S, Putz B, Sasaki Y, Takino R, Sakai K and Tamada T 1999 Functional magnetic resonance imaging of neural activity related to orthographic, phonological and lexico-semantic judgments of visually presented characters and words *Hum. Brain Mapp.* **8** 44–59

Gorodnistky I F, George J S and Rao B D 1995 Neuromagnetic imaging with FOCUSS: a recursive weighted minimum norm algorithm *Electroencephalogr. Clin. Neurophysiol.* **95** 231–51

Hämäläinen M S, Hari R, Ilmoniemi R J, Knuutila J and Lounasmaa O V 1993 Magnetoencephalography. Theory, instrumentation and applications to the noninvasive study of human brain function *Rev. Mod. Phys.* **65** 413–97

Hämäläinen M S and Sarvas J 1989 Realistic conductivity geometry model of the human head for interpretation of neuromagnetic data *IEEE Trans. Biomed. Eng.* **36** 165–71

Im C-H, An K-O, Jung H-K, Kwon H and Lee Y-H 2003 Assessment criteria for MEG/EEG cortical patch tests *Phys. Med. Biol.* **48** 2561–73

Jerbi K, Mosher J C, Nolte G, Baillet S, Garnero L and Leahy R M 2002 From dipoles to multipoles: parametric solutions to the inverse problem in MEG *Proc. Conf. on Biomagnetism—BIOMAG 2002*

Kincses W E, Braun C, Kaiser S and Elbert T 1999 Modeling extended sources of event-related potentials using anatomical and physiological constraints *Hum. Brain Mapp.* **8** 182–93

Lin Y-Y, Chang K-P, Hsieh J-C, Yeh T-C, Yu H-Y, Kwan S-Y, Yen D-J, Yiu C-H and Hari R 2003 Magnetoencephalographic analysis of bilaterally synchronous discharges in benign Rolandic epilepsy of childhood *Seizure* **12** 448–55

Lin F-H, Witzel T, Hämäläinen M S, Dale A M, Belliveau J W and Stufflebeam S M 2004 Spectral spatiotemporal imaging of cortical oscillations and interactions in the human brain *Neuroimage* **23** 582–95

Liu A K, Belliveau J W and Dale A M 1998 Spatiotemporal imaging of human brain activity using functional MRI constrained magnetoencephalography data: Monte Carlo simulations *Proc. Natl. Acad. Sci.* **95** 8945–50

Liu A K, Dale A M and Belliveau J W 2002 Monte Carlo simulation studies of EEG and MEG localization accuracy *Hum. Brain Mapp.* **16** 47–62

Malmivuo J and Plonsey R 1995 *Bioelectromagnetism* (Oxford: Oxford University Press)

Meijs J W, Peters M J, Boom H B and Lopes da Silva F H 1988 Relative influence of model assumptions and measurement procedures in the analysis of the MEG *Med. Biol. Eng. Comput.* **26** 136–42

Mosher J C, Leahy R and Lewis P 1992 Multiple dipole modeling and localization from spatio-temporal MEG data *IEEE Trans. Biomed. Eng.* **39** 541–57

Nuwer M R, Comi G, Emerson R, Fuglsang-Frederiksen A, Guerit J M, Hinrichs H, Ikeda A, Luccas F J C and Rappelsburger P 1998 IFCN standards for digital recording of clinical EEG *Electroencephalogr. Clin. Neurophysiol.* **106** 259–61

Shattuck D W and Leahy R M 2002 BrainSuite: an automated cortical surface identification tool *Med. Image Anal.* **6** 129–42

Uutela K, Hämäläinen M and Salmelin R 1998 Global optimization in the localization of neuromagnetic sources *IEEE Trans. Biomed. Eng.* **45** 716–23

Yoshinaga H, Koutroumanidis M, Shirasawa A, Kikumoto K, Ohtsuka Y and Oka E 2005 Dipole analysis in panayiotopoulos syndrome *Brain Dev.* **27** 46–51